Astronomy & Astrophysics manuscript no. 14430˙arx
April 2, 2010

LETTER TO THE EDITOR

XMMU J100750.5+125818: A strong lensing cluster at $z = 1.082^{\star,\star\star}$

A.D. Schwope[1], G. Lamer[1], A. de Hoon[1], J. Kohnert[1], H. Böhringer[2], J.P. Dietrich[3], R. Fassbender[2], J. Mohr[4,2,5], M. Mühlegger[2], D. Pierini[2], G.W. Pratt[6,2], H. Quintana[7], P. Rosati[8], J. Santos[9], and R. Šuhada[2]

[1] Astrophysikalisches Institut Potsdam, An der Sternwarte 16, 14482 Potsdam, Germany
[2] Max-Planck-Institut für Extraterrestrische Physik, 85748 Garching, Germany
[3] Physics Department and Michigan Center for Theoretical Physics, University of Michigan, 450 Church St, Ann Arbor, MI 48109-1040, USA
[4] Department of Physics, Ludwig-Maximilians-Universität, Scheinerstraße 1, 81679 Munich, Germany
[5] Excellence Cluster Universe, Boltzmannstr. 2, 85748 Garching, Germany
[6] Laboratoire AIM, IRFU/Service d'Astrophysique - CEA/DSM - CNRS - Université Paris Diderot, Bât. 709, CEA-Saclay, F-91191 Gif-sur-Yvette Cedex, France
[7] Departamento de Astronomia y Astrofisica, Pontificia Universidad Catolica de Chile, Casilla 306, Santiago, 22, Chile
[8] European Southern Observatory, Karl-Schwarzschild-Strasse 2, 85748 Garching, Germany
[9] INAF-Osservatorio Astronomico di Trieste, via Tiepolo 11, 34131 Trieste, Italy

Received / Accepted

ABSTRACT

We report on the discovery of the X-ray luminous cluster XMMU J100750.5+125818 at redshift 1.082 based on 19 spectroscopic members, which displays several strong lensing features. SED modeling of the lensed arc features from multicolor imaging with the VLT and the LBT reveals likely redshifts ∼2.7 for the most prominent of the lensed background galaxies. Mass estimates are derived for different radii from the velocity dispersion of the cluster members, $M_{200} \simeq 1.8 \times 10^{14}\,M_\odot$, from the X-ray spectral parameters, $M_{500} \simeq 1.0 \times 10^{14}\,M_\odot$, and the largest lensing arc, $M_{SL} \simeq 2.3 \times 10^{13}\,M_\odot$. The projected spatial distribution of cluster galaxies appears to be elongated, and the brightest galaxy lies off center with respect to the X-ray emission indicating a not yet relaxed structure. XMMU J100750.5+125818 offers excellent diagnostics of the inner mass distribution of a distant cluster with a combination of strong and weak lensing, optical and X-ray spectroscopy.

Key words. galaxies: clusters of galaxies – X-rays: clusters of galaxies

1. Introduction

A crucial prerequisite for the use of clusters of galaxies for cosmological studies is the knowledge of the scaling relations between cluster mass and an observable proxy, such as X-ray luminosity, or X-ray gas temperature. These relations must be calibrated at varying redshifts, using theoretical modeling and hydrosimulations, or simply empirical relations. Clusters at low and intermediate redshifts are bright enough in X-rays to measure the total gravitating mass by deprojecting their temperature and density profiles. This is currently difficult for clusters beyond $z \sim 1$ and subject to large statistical errors (e.g. Rosati et al. 2004). In this high redshift regime, independent mass estimates based on gravitational lensing (both in the weak and the strong regimes) have long been invoked as the most effective method for calibrating cluster masses. In particular, mass measurements based on multiple strong lensing features are highly robust. Although such measurements are possible only in the central region of the cluster, they are independent of model assumptions and can help to break the mass-sheet degeneracy of parameter-free weak-lensing mass-reconstructions.

To obtain a well-defined sample of clusters at high redshift, $z > 0.8$, we have started the XDCP (XMM-Newton Distant Cluster Project, Böhringer et al. 2005; Fassbender et al. 2008; Mullis et al. 2005) based on archival XMM-Newton X-ray data. The XDCP has been very successful, so far providing 18 clusters at $z > 0.8$ and 10 clusters with $z > 1$ including five redshift confirmations from other projects (for selected results see e.g. Fassbender et al. 2008; Santos et al. 2009; Rosati et al. 2009).

Here we report the discovery of a distant strong lensing cluster of galaxies at redshift $z = 1.082$ which shows a giant arc and other arc-like features interpreted as gravitationally lensed images of more distant, background objects. We study the properties of the lensing cluster and the lensed galaxies on the basis of available optical and X-ray imaging and spectroscopy.

Throughout this paper we use a standard ΛCDM cosmology with parameters $H_0 = 71\,\mathrm{km\,s^{-1}\,Mpc^{-1}}$, $\Omega_M = 0.27$, and $\Omega_\Lambda = 0.73$, which gives a scale of 8.188 kpc arcsec^{-1} at redshift 1.082. All magnitudes in this paper are given in the AB system.

2. Observations, analysis and results

2.1. XMM-Newton X-ray observations

XMMU J100750.5+125818 (hereafter XMMU J1007) was found serendipitously as an extended X-ray source in our systematic search for distant clusters of galaxies. The cluster candidate was detected in a field with nominal exposure time of

Send offprint requests to: A. Schwope, e-mail: aschwope@aip.de

⋆ Based on observations made with ESO Telescopes at the La Silla or Paranal Observatories under programmes 78.A-0265 and 80.A-0659

⋆⋆ Based on observations obtained with XMM-Newton, an ESA science mission with instruments and contributions directly funded by ESA Member States and NASA

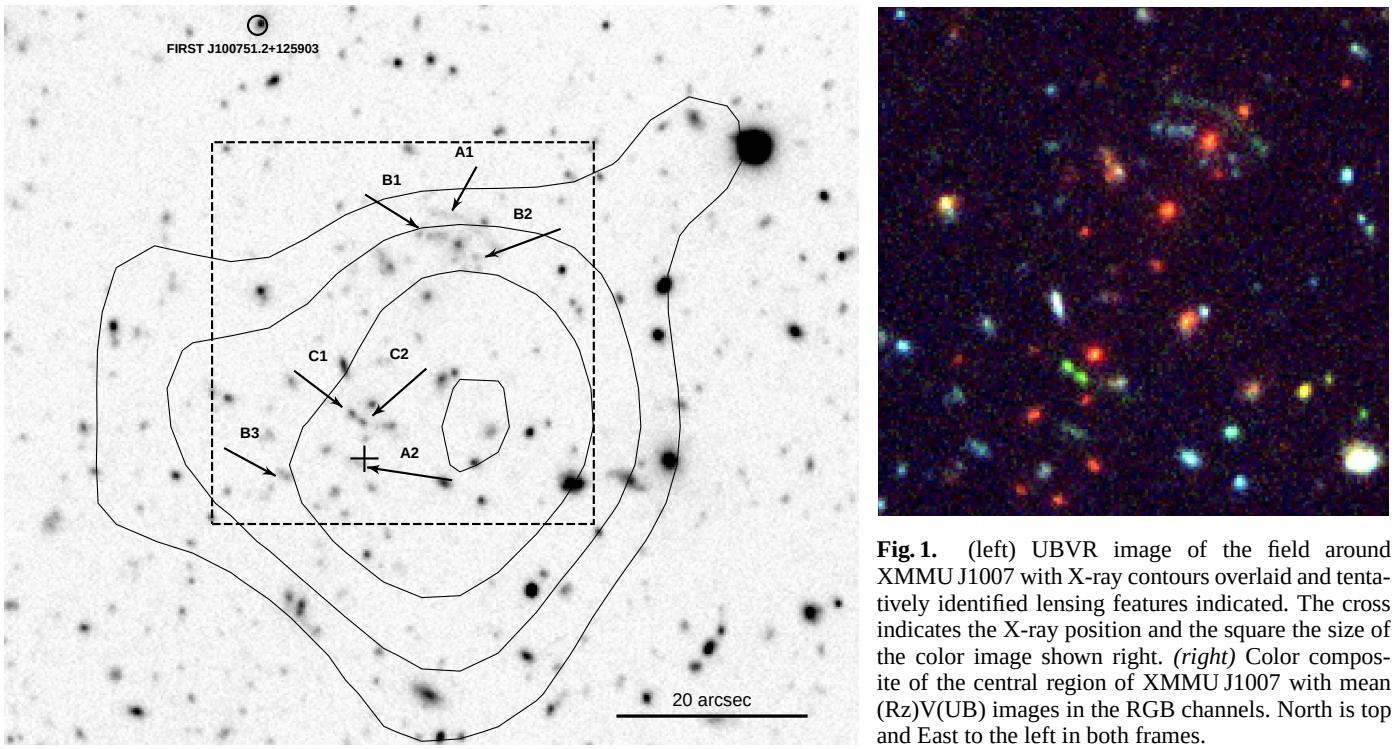

Fig. 1. (left) UBVR image of the field around XMMU J1007 with X-ray contours overlaid and tentatively identified lensing features indicated. The cross indicates the X-ray position and the square the size of the color image shown right. *(right)* Color composite of the central region of XMMU J1007 with mean (Rz)V(UB) images in the RGB channels. North is top and East to the left in both frames.

22.2ksec at an off-axis angle of 11.7′ (OBSID: 0140550601). Following Pratt & Arnaud (2003), time intervals with high background were excluded by applying a two-step flare cleaning procedure firstly in a hard energy band (10 − 14 keV) and subsequently in the 0.3 − 10 keV band, after which 21.4 ksec of clean exposure time remained for the two MOS cameras and 18.0 ksec for the PN instrument.

Images and exposure maps were created in the 0.35−2.4 keV detection band, which was chosen to maximize the signal-to-noise ratio of the X-ray emission of massive galaxy clusters at $z > 0.8$ compared to the background components (Scharf 2002). Source detection was performed with the SAS task `eboxdetect` followed by the maximum likelihood fitting task `emldetect` for the determination of source parameters. XMMU J1007 was found as an extended X-ray source with low surface brightness at position $\alpha(2000) = 10^h07^m50\overset{s}{.}5, \delta(2000) = +12°58'18\overset{''}{.}1$ with a total of about 200 source photons and a core radius of 24″ at a significance level of $\mathrm{DET_{ML}} \sim 42$ and an extent likelihood of $\mathrm{EXT_{ML}} \sim 24$[1]. XMMU J1007 is not listed in the 2XMM catalog (Watson et al. 2009), since its detection likelihood after the first step of the detection chain (`eboxdetect`) remained below the threshold to perform the second step (`emldetect`). It was revealed as a cluster candidate in this work, however, owing to the use of a different detection band and by lowering the detection threshold to perform `emldetect`.

2.2. Optical imaging with VLT/FORS2 and LBT/LBC

Neither DSS nor the SDSS revealed a convincing counterpart to the unique X-ray source XMMU J1007[2]. The field containing XMMU J1007 was thus observed with FORS2 at the VLT in January/February 2007 through ESO filters R_SPECIAL+76 and z_GUNN+78 with total integration times of 1920 s and 960 s, respectively. The combination of filters was chosen to allow an unambiguous redshift determination up to $z \sim 0.9$ through the identification of a cluster red sequence (CRS).

All the imaging data of this paper were reduced with an AIP-adaptation of the GaBoDS-pipeline described in Erben et al. (2005). It comprises all the pre-processing steps (bias- and flatfield-, and fringe-correction) as well as super-flat correction, background subtraction, and creation of a final mosaic image using SWarp and ScAMP (Bertin 2006).

The photometric calibration of the *R*-band image was achieved through observations of Stetson (2000) standard fields, the photometry of the z-band image was tied to the SDSS. The non-standard z-band cut-on filter in use at the VLT leads to an estimated systematic calibration uncertainty of 0.05 mag.

The measured image seeing of the VLT R- and z-band images is 0.″7 and 0.″56, respectively. Object catalogues were generated with SExtractor (Bertin & Arnouts 1996) in double image mode. The magnitudes of catalogued objects were corrected for Galactic foreground extinction. From the observed drop of the number-flux relations with respect to a power-law expectation we estimate a 50% completeness of the catalogues of $R_{\rm lim} \sim 25.9$ and $z_{\rm lim} \sim 24.6$. Following Mullis et al. (2005, and its erratum) we used fixed apertures with diameter $3.5 \times \mathrm{FWHM_{seeing}}$ to determine object colors.

A mere two-band false-color composite of the VLT imaging data proved sufficient to locate an overdensity of red, early type galaxies at the position of the extended X-ray emission. Color- and location-selected possible cluster members form a red sequence in the color-magnitude diagram of Fig. 2. The red sequence color was estimated from the average color of all galaxies

[1] $\mathrm{DET_{ML}}$, $\mathrm{EXT_{ML}}$: detection likelihood and extent likelihood of the source, $L = -\ln P$, where P is the probability the detection (the extent) is spurious due to a Poissonian fluctuation

[2] We regard the NVSS radio source NVSS J100751+125901 at $10^h07^m51\overset{s}{.}3, +12°59'01''$ (J2000.0), marked in Fig. 1, and confirmed to be point-like by FIRST ($10^h07^m51\overset{s}{.}289s, +12°59'3\overset{''}{.}34$) with an integrated flux of 5.59 ± 0.19 mJy (positional offset of 48″) as unrelated to the X-ray source

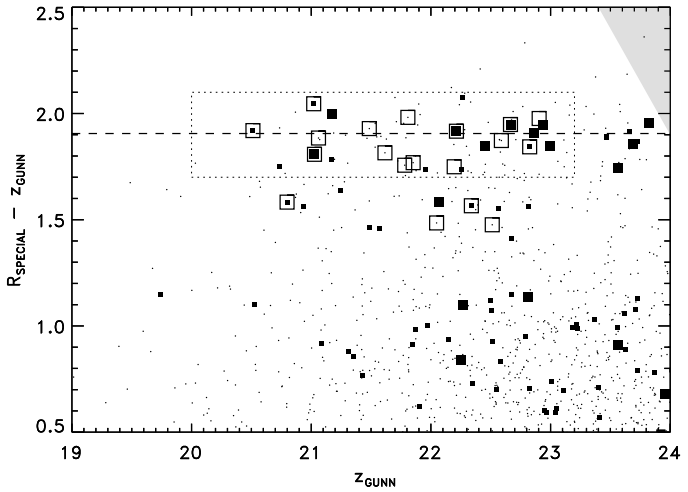

Fig. 2. Color-magnitude diagram of XMMU J1007. The size of the symbols encodes vicinity to the X-ray center of the cluster (within 30″, and 60″ and beyond). Objects within the dotted box were used to estimate the color of the red sequence (solid horizontal line). Objects framed with squares are spectroscopically confirmed cluster members. The shaded region top right indicates > 50% incompleteness.

within 30″of the X-ray position (see box in Fig. 2), $R-z = 1.91$, which hints to a cluster redshift beyond ∼0.9.

Further imaging observations were performed with the Large Binocular Telescope (LBT) equipped with the Large Binocular Camera (LBC) through Bessel B,V filters and the U_{spec} filter. Table A.1 lists the details of the LBT imaging observations.

The photometric zeropoints for the LBC images were derived by using the SDSS photometry of stellar objects in the field.

A multi-color composite of the center of the field including VLT/FORS2- and LBT/LBC-data is shown in Fig. 1 with X-ray contours overlaid. Residual astrometric uncertainties in the XMM-Newton X-ray image were removed on the basis of identified X-ray point sources in the FORS- and LBT-images, respectively.

The cluster has its brightest galaxy (BCG) at position $\alpha = 10^{\rm h}07^{\rm m}49.9^{\rm s}$ and $\delta = +12°58'40''$ between structures B1 and B2 (see Fig. 1), i.e. away from the apparent center of the galaxy distribution by about 20″ and away from the X-ray position. The BCG has an apparent magnitude $z_{\rm BCG} = 20.51 \pm 0.06$, an osberved color $(R-z)_{\rm BCG} = 1.92 \pm 0.08$ and an absolute magnitude $M_{\rm BCG,z} = -23.8$.

The spatial distribution of galaxies that form the red sequence of Fig. 2 appears stretched in a band from SSE to NNW with a centroid about 10″ away from the centroid of the cluster X-ray emission. However, the best-fit X-ray position (Maximum Likelihood fit of an assumed β-profile folded with the PSF of the X-ray telescope) lies well within the galaxy assembly (see Fig. 1).

2.3. Optical spectroscopy

Multi-object spectroscopy of XMMU J1007 was performed with VLT/FORS2 using the MXU option in December 2007 and January 2008. One mask was prepared targeting 37 candidate objects selected as possible cluster members based on color and stellarity index. Individual exposures of 1308 s were combined to yield a total integration time per object of 2.9 h. Spectra were obtained with grism 300I; they cover the wavelength range 6000 – 11000 Å with a scale of 3.2 Å/pixel at the chosen 2 × 2 binning.

We obtained 32 classifiable spectra (among them two late-type stars) and measured the redshifts of galaxies by fitting double Gaussians with fixed wavelength ratio and same width to the Ca H&K lines. The measured redshifts together with coordinates, brightness, and color of the 32 objects are listed in Table A.2 and marked on Fig. A.3 (appendix).

We found 19 concordant redshifts between 1.075 and 1.088 with a weighted mean of 1.08103 and a median of 1.08207. We assume a cluster redshift of 1.082 in the following. The redshifts in this interval are Gaussian distributed, a one-sample KS-test reveals a probability of rejecting the null hypothesis of 1.3%. The distribution of all redshifts is shown in Fig. A.1. Following Danese et al. (1980) we calculate a line-of-sight velocity dispersion of $\sigma_{\rm p} = 572\,{\rm km\,s^{-1}}$with a 90% confidence range between $437\,{\rm km\,s^{-1}}$and $780\,{\rm km\,s^{-1}}$.

Although the cluster does not appear to be relaxed, we may estimate a mass on the virial assumption. Using $R_{200} = \sqrt{3}/10\sigma/H(z)$, $M_{200} = 4/3\pi R_{200}^3 \times 200\rho_c$ (Carlberg et al. 1997), we obtain $R_{200} = 790^{+280}_{-185}\,{\rm kpc}$, and $M_{200} = 1.8^{+2.8}_{-1.0} \times 10^{14}\,{\rm M_\odot}$ where the given errors correspond to the 90% confidence interval of the velocity dispersion. Using the dark matter halo virial scaling relation by Evrard et al. (2008) instead, one obtains $M_{200} = 1.2^{+1.8}_{-0.7} \times 10^{14}\,{\rm M_\odot}$.

2.4. X-ray spectroscopy

X-ray spectra were extracted from the calibrated photon event lists of all three EPIC cameras onboard XMM-Newton. An aperture with 60″ radius (∼500 kpc at the cluster distance) was used to extract source and background photons. The X-ray spectrum of XMMU J1007 contains ∼200 net photons in the full XMM-band after background subtraction.

An attempt was made to constrain the plasma temperature with a thin thermal plasma model (a MEKAL model in XSPEC terms, Mewe et al. 1985). The column density of absorbing matter was fixed to its galactic value, $N_{\rm H} = 3.7 \times 10^{20}\,{\rm cm^{-2}}$, the metal abundance to $Z = 0.3 Z_\odot$, and the redshift to $z = 1.082$.

Despite fixing these parameters, the X-ray temperature could only be roughly constrained. The fit shown in Fig. A.2 converges at a temperature of $T = 5.7\,{\rm keV}$ ($kT > 2.05\,{\rm keV}$ with 90% confidence) implying a bolometric X-ray luminosity of $L_{\rm X} = 1.3 \times 10^{44}\,{\rm erg\,s^{-1}}$ ($L_{\rm X} > 0.8 \times 10^{44}\,{\rm erg\,s^{-1}}$ at 90% confidence, $L_{\rm X}(0.5-2.0\,{\rm keV}) = 4 \times 10^{43}\,{\rm erg\,s^{-1}}$).

Following Pratt et al. (2009) we estimate the cluster mass using the luminosity-mass scaling relation. We use their BCES orthogonal fit to the Malmquist-bias corrected L-M relation, assume self-similar evolution, $h(z)^{-7/3}$, and obtain $M_{500} = 1.0 \times 10^{14}\,{\rm M_\odot}$ (assuming our aperture covers R_{500}). If we instead use the temperature-mass relation of Vikhlinin et al. (2009) we find $M_{500} = 2.1 \times 10^{14}\,{\rm M_\odot}$ with a lower limit of $M_{500} = 4.3 \times 10^{13}\,{\rm M_\odot}$.

2.5. Lensing properties

Our follow-up imaging observations confirmed the existence of lensing arcs and further lensing features in the image. We used the imaging data in the five passbands (UBVRz) from the LBT and the VLT to calculate photometric redshifts of the lensed background objects. Due to the distorted morphology of the lensing arcs we manually defined apertures matching the shape of each feature. The fluxes of the objects were then extracted using

the same aperture in each image and converted to AB magnitudes.

Table 1. Photometric redshifts of lensing features. All redshifts were forced to be larger than the cluster redshift.

Image	V_{AB}	z_{phot}	z range (90%)
A1	24.3	2.72	2.63 - 2.82
A2	25.1	2.63	2.54 - 2.73
B1	24.5	1.39	1.35 - 1.52
B2	25.7	1.63	1.08 - 1.74
B3	24.7	1.94	1.70 - 2.12
C1	24.3	3.36	2.98 - 3.54
C2	23.6	3.20	2.70 - 3.40

We used the publicly available `hyperz` code (Bolzonella et al. 2000) to compare the spectral energy distributions of the lensing features with the synthetic galaxy SEDs from Bruzual & Charlot (1993). The parameters for the construction of the SED data cube were galaxy class, star forming age, internal reddening , and redshift. For the lens features we allowed only redshifts beyond the redshift of the cluster ($z = 1.082$) and combinations of age and redshift consistent with our adopted cosmological parameters.

Table 1 shows the results of the SED fitting for the image components as indicated in Fig. 1. Column (2) gives the best fitting photometric redshift and column (3) the 90% confidence limits of the redshift within the best fitting SED template.

The resulting photometric redshifts confirm our tentative identification of multiple lensed components. Components A1/A2 and C1/C2 are likely to be images of the same background objects at $z \sim 2.7$ and $z \sim 3$, respectively. The situation is less clear for components B1, B2, and B3, where the uncertainties in the photometric redshifts are large.

We estimate a lensing mass assuming a circularly symmetric lens (a special case is the singular isothermal sphere – SIS). The projected mass inside a tangential arc then becomes $M(\theta) = \Sigma_{cr}\pi(D_d\theta)^2 \simeq 1.1 \times 10^{14} \left(\frac{\theta}{30''}\right)\left(\frac{D}{1\mathrm{Gpc}}\right) \mathrm{M}_\odot$. The effective distance D becomes $D = \frac{D_d D_{ds}}{D_s} = 724\,\mathrm{Mpc}$ for $z_d = 1.082$ and $z_s = 2.7$.

Difficulties arise from the faintness of the lensing features and from the badly determined cluster center. A trace of the feature A1 implies an Einstein radius of $\theta \sim 8'' - 9''$ and a corresponding mass of $(2.3 \pm 0.4) \times 10^{13}\,\mathrm{M}_\odot$ (a 15% uncertainty in radius is assumed). If one uses uses the distance between A1 and the X-ray center (21.″5) instead, the mass inside this ring becomes $5.7 \times 10^{13}\,\mathrm{M}_\odot$.

3. Discussion and conclusions

We have presented results of an initial study of the X-ray selected cluster XMMU J1007. We determine a redshift of $z = 1.082$ based on 19 spectroscopic confirmed members. As most prominent property, the cluster shows several strong lensing features. It is an optically rich cluster; the absence of a dominant BCG and the elongated distribution of member galaxies suggest a not yet relaxed structure. The bolometric X-ray luminosity is $L_X \approx 1.3 \times 10^{44}$ergs/s.

Estimates of the cluster mass were obtained via strong lensing, X-ray spectroscopy and the velocity dispersion of member galaxies; the values obtained at different radii are summarized in Fig. 3. One obtains overlapping error bars for the mass at $\sim R_{200}$ (∼virial radius) and at $\sim R_{500}$ (∼X-ray aperture) due to insufficient data and uncertainties in the scaling relations. If one takes

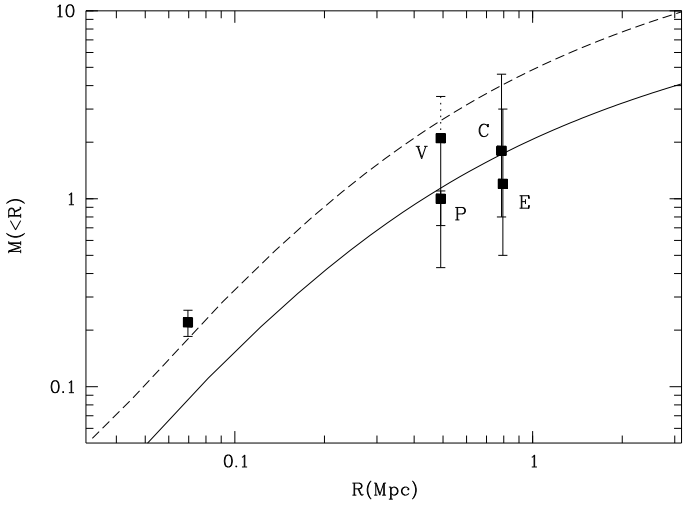

Fig. 3. Comparison of different mass estimates for XMMU J1007 in units of $10^{14}\,\mathrm{M}_\odot$. Labels indicate results based an scaling relations by Vikhlinin et al. (2009); Pratt et al. (2009); Carlberg et al. (1997); Evrard et al. (2008). The dashed and solid lines indicate universal density profiles (Navarro et al. 1997) with concentration parameters of 3.86 and 3.45 for virial masses 1.8 and $4.6 \times 10^{14}\,\mathrm{M}_\odot$ at an assumed $R_{vir} = 780\,\mathrm{kpc}$, respectively (Bullock et al. 2001).

$M_{vir} \simeq M_{200} = 1.8 \times 10^{14}\,\mathrm{M}_\odot$ at face value, our strong lensing result seems to be discrepant with an NFW-profile. All data can be made compliant at a mass of about $4 \times 10^{14}\,\mathrm{M}_\odot$, higher than but not excluded by the velocity dispersion and the X-ray temperature, whereas a weak-lensing mass is key to fix the halo profile at large radii, a deep X-ray observation is necessary to determine the X-ray morphology and the gas temperature. The modelling of the strong lensing system is important to probe the inner density profile.

Interestingly, in a study of a complete sample of 12 MACS clusters Zitrin et al. (2010) find the observed Einstein radii to be larger and hence the central density of cluster higher than predicted by simulations and interpret their finding as a challenge to cluster formation in a ΛCDM model. They invoke the possibility that the formation of clusters started at earlier epochs than currently assumed, leading to higher central Dark Matter concentrations. Also, Jee et al. (2009) suggest this scenario as a possible explanation for the discovery of unexpectedly massive clusters at $z >\sim 1$ in the moderate survey volume probed by the XMM-Newton serendipitous surveys (like e.g. XMMU J2235-2557 and 2XMM J083026+524133, Mullis et al. 2005; Lamer et al. 2008; Rosati et al. 2009). However, in a recent study of the strong lensing clusters in the Mare Nostrum Universe, Meneghetti et al. (2010, subm. to A&A) find the concentration and the X-ray luminosity to be biased high, and an excess of kinetic energy within the virial radius among the strong lensing clusters. XMMU J1007 is a highly suited target to confront theory and observation.

The elongated distribution of the cluster member galaxies may point to the principal direction of merging or accretion of XMMU J1007 (Dubinski 1998). The merging hypothesis is consistent with the system being a strong lens (see e.g. the chain distribution of the brightest member galaxies in the strong-lensing main component of the Bullet Cluster, Bradač et al. 2006). On the other hand, the chain distribution of the bright member galaxies of XMMU J1007 may suggest that the infall of these galaxies happens along filaments with small impact parameters, so that dynamical friction is particularly efficient in dragging them to

the cluster center and originate a dominant BCG within a short time (D'Onghia et al. 2005). In analogy with the formation of fossil galaxy groups studied by the latter authors, the small impact parameters of the filaments may lead to an early assembly of the gas in the center, thus to an early start of its cooling. The resulting system may exhibit an enhanced X-ray luminosity with respect to the optical one. This efficient, early formation may offer an alternative explanation to merging for the reason why particularly X-ray luminous clusters with chain distribution of their bright members are detected at high redshifts.

Acknowledgements. We thank J. Wambsganss for providing software code describing the lensing geometry. We thank S. Schindler and W. Kausch for an early analysis of the lensing features. HQ thanks the FONDAP Centro de Astrofisica for partial support. This work was supported by the DFG under grants Schw 536/24-2 and BO 702/16-3, and the German DLR under grant 50 QR 0802.

We thank our referee, Florence Durret, for constructive criticism.

Based on data acquired using the Large Binocular Telescope (LBT). The LBT is an international collaboration among institutions in the United States, Italy, and Germany. LBT Corporation partners are: The University of Arizona on behalf of the Arizona university system; Istituto Nazionale di Astrofisica, Italy; LBT Beteiligungsgesellschaft, Germany, representing the Max-Planck Society, the Astrophysical Institute Potsdam, and Heidelberg University; The Ohio State University, and the Research Corporation, on behalf of The University of Notre Dame, University of Minnesota, and University of Virginia.

References

Bertin, E. 2006, in Astronomical Society of the Pacific Conference Series, Vol. 351, Astronomical Data Analysis Software and Systems XV, ed. C. Gabriel, C. Arviset, D. Ponz, & S. Enrique, 112–115
Bertin, E. & Arnouts, S. 1996, A&AS, 117, 393
Böhringer, H., Mullis, C., Rosati, P., et al. 2005, The Messenger, 120, 33
Bolzonella, M., Miralles, J.-M., & Pelló, R. 2000, A&A, 363, 476
Bradač, M., Clowe, D., Gonzalez, A. H., et al. 2006, ApJ, 652, 937
Bruzual, A. & Charlot, S. 1993, ApJ, 405, 538
Bullock, J. S., Kolatt, T. S., Sigad, Y., et al. 2001, MNRAS, 321, 559
Carlberg, R. G., Yee, H. K. C., Ellingson, E., et al. 1997, ApJ, 485, L13
Danese, L., de Zotti, G., & di Tullio, G. 1980, A&A, 82, 322
D'Onghia, E., Sommer-Larsen, J., Romeo, A. D., et al. 2005, ApJ, 630, L109
Dubinski, J. 1998, ApJ, 502, 141
Erben, T., Schirmer, M., Dietrich, J. P., et al. 2005, Astronomische Nachrichten, 326, 432
Evrard, A. E., Bialek, J., Busha, M., et al. 2008, ApJ, 672, 122
Fassbender, R., Böhringer, H., Lamer, G., et al. 2008, A&A, 481, L73
Jee, M. J., Rosati, P., Ford, H. C., et al. 2009, ApJ, 704, 672
Krumpe, M., Lamer, G., Corral, A., et al. 2008, A&A, 483, 415
Lamer, G., Hoeft, M., Kohnert, J., Schwope, A., & Storm, J. 2008, A&A, 487, L33
Mewe, R., Gronenschild, E. H. B. M., & van den Oord, G. H. J. 1985, A&AS, 62, 197
Mullis, C. R., Rosati, P., Lamer, G., et al. 2005, ApJ, 623, L85
Navarro, J. F., Frenk, C. S., & White, S. D. M. 1997, ApJ, 490, 493
Pratt, G. W. & Arnaud, M. 2003, A&A, 408, 1
Pratt, G. W., Croston, J. H., Arnaud, M., & Böhringer, H. 2009, A&A, 498, 361
Rosati, P., Tozzi, P., Ettori, S., et al. 2004, AJ, 127, 230
Rosati, P., Tozzi, P., Gobat, R., et al. 2009, A&A, 508, 583
Santos, J. S., Rosati, P., Gobat, R., et al. 2009, A&A, 501, 49
Scharf, C. 2002, ApJ, 572, 157
Stetson, P. B. 2000, PASP, 112, 925
Vikhlinin, A., Burenin, R. A., Ebeling, H., et al. 2009, ApJ, 692, 1033
Watson, M. G., Schröder, A. C., Fyfe, D., et al. 2009, A&A, 493, 339
Zitrin, A., Broadhurst, T., Barkana, R., Rephaeli, Y., & Benitez, N. 2010, ArXiv e-prints

Appendix A: Supplementary electronic material

This appendix gives further detailed information about optical observations, the X-ray spectrum, the redshift distribution and the brightness of spectroscopically classified objects in the field of XMMU J1007.

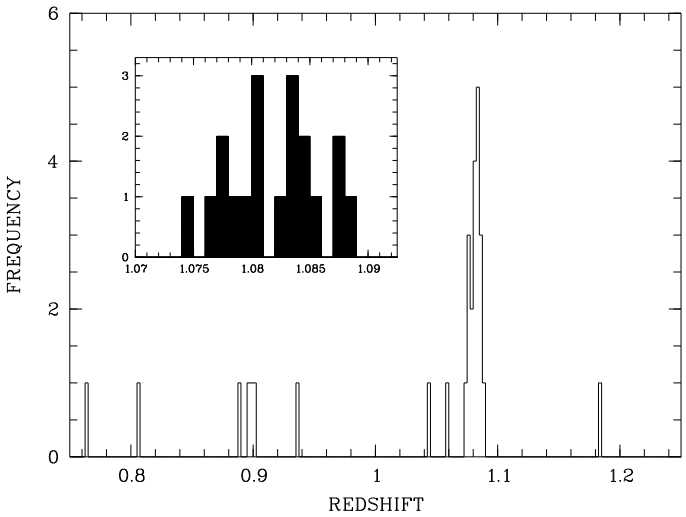

Fig. A.1. Redshift distribution of galaxies in the field of XMMU J1007 observed with VLT-FORS2-MXU (see Table A.2). The inset is a blow-up comprising the redshift range covered by likely cluster members.

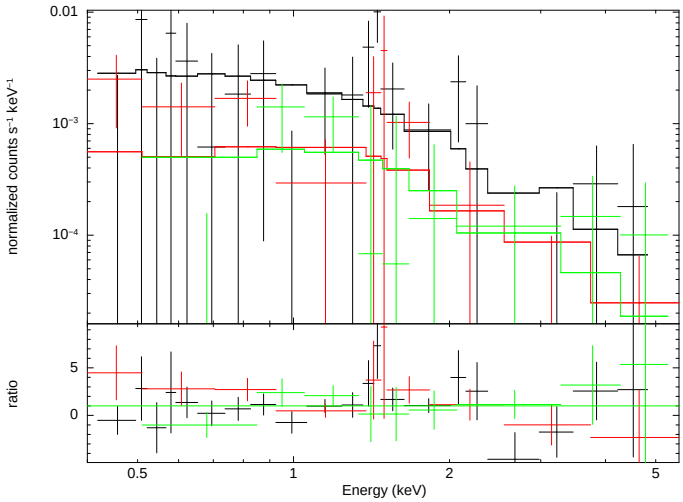

Fig. A.2. XMM-Newton X-ray spectrum of XMMU J1007 (EPIC-pn in black, EPIC-MOS in red and green). A thin thermal plasma model (the so-called MEKAL-model in the X-ray spectral fitting package *XSPEC*) was fitted to the data. Fit optimisation was achieved by using the Cash-statistic with one count per bin (Krumpe et al. 2008). It does not, however, provide a goodness-of-fit statistic. The fit suggests a cluster temperature of $T = 5.7$ keV ($kT > 2.05$ keV with 90% confidence). The temperature is not constrained towards high values. The bolometric X-ray luminosity of this model is $L_X = 1.3 \times 10^{44}$ ergs s^{-1}.

Table A.1. LBT image parameters

filter	date	exposure	seeing	zeropoint
U_{spec}	31-Dec-2008	1200 s	0.″65	26.73
B_{Bessel}	31-Dec-2008	1070 s	0.″75	27.41
V_{Bessel}	31-Dec-2008	1200 s	0.″78	28.01

Table A.2. Spectroscopically confirmed cluster member galaxies (upper part) and non-member galaxies targeted by VLT-MOS spectroscopy sorted by increasing z-band magnitude. The 2nd to last column lists the positional offset with respect to the assumed cluster center at the nominal X-ray position (R.A. 151.9604°, Decl. 12.9717°). A colon indicates a less secure measurement, which may be subject to future adjustment.

ID	R.A. J2000 (deg)	Decl. J2000 (deg)	z (mag)	R–z (mag)	redshift z	δz	Distance (arcsec)	
1-10	151.95762	12.97789	20.51	1.92	1.08423	0.00012	24.1	
1-5	151.96234	12.96729	20.80	1.59	1.08086	0.00012	17.8	
1-9	151.95854	12.97640	21.02	2.05	1.08709	0.00021	17.8	
1-8	151.95809	12.97400	21.03	1.81	1.07712	0.00078	11.3	
1-19	151.91809	13.00307	21.06	1.89	1.07834	0.00016	187.0	
1-20	151.92177	13.00492	21.49	1.93	1.08340	0.00014	181.3	
2-14	151.96438	12.95042	21.62	1.82	1.08715	0.00008	77.9	
2-5	151.91762	12.92344	21.78	1.76	1.08309	0.00011	229.7	
1-14	151.95837	12.98867	21.81	1.98	1.07465	0.00009	61.5	
1-21	151.92233	13.00835	21.85	1.77	1.08207	0.00010	188.3	
1-16	151.92898	12.99330	22.05	1.48	1.07995	0.00009	135.0	
2-9	151.92196	12.93457	22.19	1.75	1.07749	0.00009	189.9	
1-7	151.96153	12.97194	22.21	1.92	1.08463	0.00013	4.6	
1-3	151.96457	12.96373	22.34	1.57	1.08069	0.00022	32.6	
2-1	151.91657	12.91210	22.51	1.48	1.08085:	0.00066	263.7	
1-15	151.94809	12.99093	22.59	1.88	1.08370	0.00017	81.5	
1-6	151.96098	12.97008	22.67	1.95	1.07673	0.00017	6.5	
1-2	151.956	12.96175	22.83	1.85	1.08538:	0.00033	39.1	
1-13	151.95492	12.98622	22.90	1.98	1.08834:	0.00020	55.6	
1-23	151.97453	13.01627	18.74	3.16	0.0	0.0	167.9	late-type star
1-11	151.94881	12.98072	20.06	2.14	0.0	0.0	52.0	late-type star
1-12	151.96350	12.98431	20.74	1.75	0.89789	0.00022	46.7	[OII]
1-1	151.94980	12.95957	20.94	1.57	1.05870	0.00021	57.4	
2-11	151.94960	12.94159	21.25	1.47	0.88879	0.00015	114.8	[OII]
1-18	151.98341	12.99842	21.87	1.80	1.18291	0.00008	125.6	
2-3	151.95777	12.91942	22.19	1.86	1.03811:	0.00011	188.4	
1-22	151.96277	13.01301	22.21	1.35	0.80748	0.00013	148.9	[OII]
2-2	151.96559	12.91600	22.24	1.42	0.89511	0.00021	201.3	
2-7	151.93620	12.92835	22.43	1.62	0.90020	0.00027	177.6	
2-8	151.97170	12.93165	22.58	1.82	1.04382:	0.00020	149.5	
2-6	151.91717	12.92623	22.68	1.36	0.76364	0.00014	223.1	
2-10	151.96192	12.93803	23.73:	0.54	0.93729	0.00019	121.3	

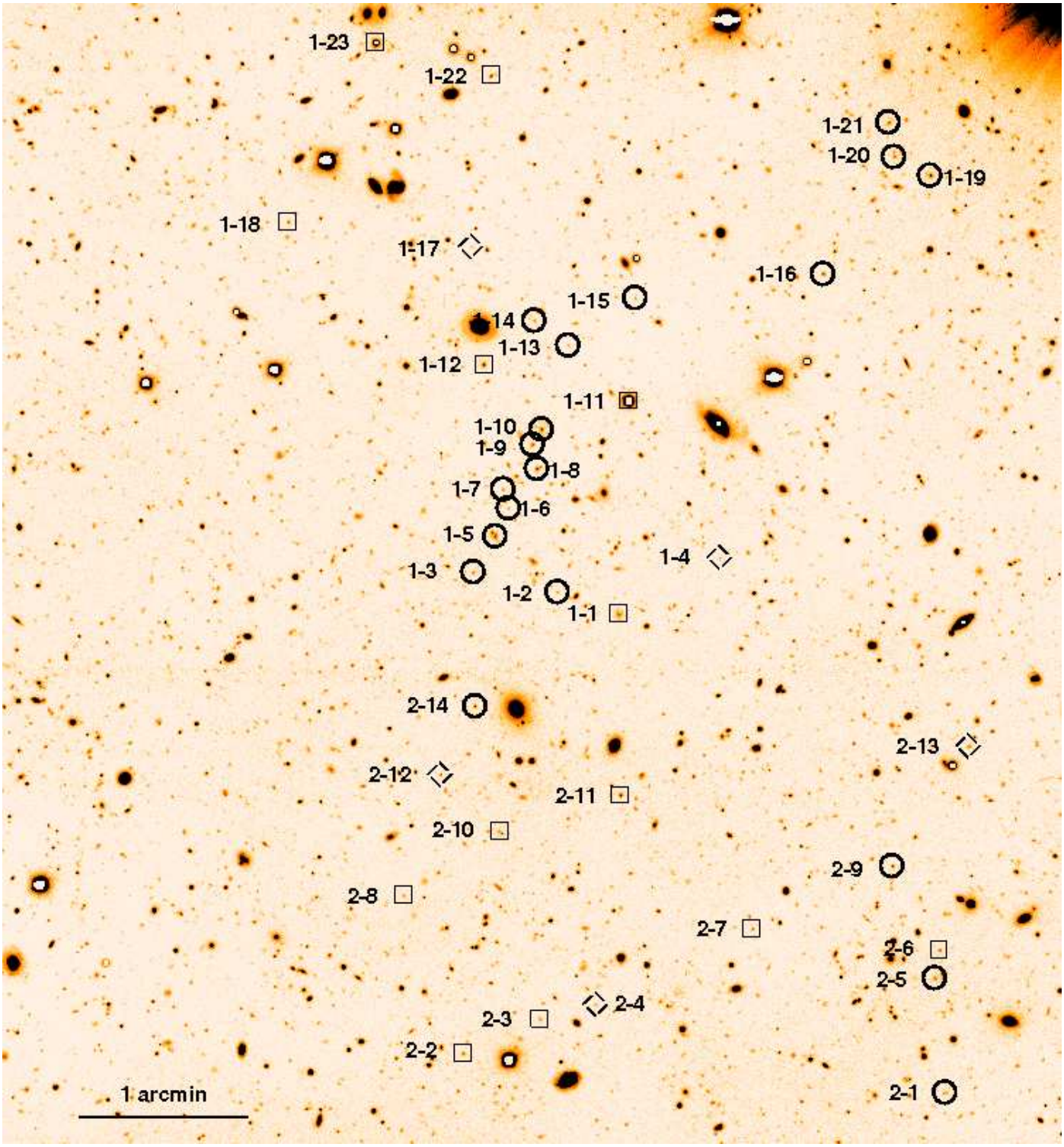

Fig. A.3. VLT/FORS2 R-band image with slit positions identified (North is top, East to the left). Labels are the same as in the first column of Table A.2. Likely cluster members are encircled, unrelated classified objects (lower section of Table A.2) are framed with squares, objects that were positioned on slits but could not yet be classified are framed with rhombs.